Non-stereoscopic 3D particle tracking velocimetry for full scale rooms

P.H. Biwole, G. Krauss, J-J. Roux, G. Rusaouen
Centre de Thermique de Lyon
CNRS-UMR 5008, INSA-Lyon, Université de Lyon
Villeurbanne, France.

E. Favier
Diagnostic et Imagerie des Procédés Industriels
Ecole Nationale d'Ingénieurs de St-Etienne
St-Etienne, France.

ABSTRACT

We are building a particle tracking system for the measurement of convective heat transfers and pollutants displacements in full scale rooms. To increase the depth of the zone of interest, the system is non stereoscopic and do not use laser light. The flow is seeded with 3mm-large neutrally buoyant helium filled soap bubbles. Illumination is provided by white continuous light. The seeded flow (air) is recorded by 3 high-speed digital video cameras located along three different planes. The experiment is taking place in a 3.1*3.1*2.5m^3 (W*D*H) test room whose boundary conditions and inner values like temperature, air velocity and solar radiation can be imposed and monitored. A specially designed tracking algorithm has been built and is being tested. The main features of the algorithm are described in this paper. Especially, our procedure to adress the correspondance problem by identifying individual particles thanks to their 3D coordinates is explained. Some early results are shown.

Keywords: object recognition, 3D reconstruction, tracking, flow visualization

1. INTRODUCTION

The research on pollutants displacement and on the low-speed interactions between airflow and heat sources in rooms is confronted to the lack of reliable and accurate 3D quantitative measurement techniques. This is a basic and long-standing problem in indoor air quality and environmental research.

Most experimental studies of the airflow field in rooms use traditional systems of metrology, such as hot wire anemometry or laser Doppler anemometry sometimes completed by the technique of the tracer gases. The disadvantages of these traditional methods are manifold. Hot wire anemometry cannot achieve 3D quantitative measurements of air speeds lower than 10 cm/s, which is the limit of precision of the probes. Unfortunately, in the majority of actual configurations, speeds of air in the zone of occupation are lower than this value. Moreover, measurement of low-speed ascendant flows with hot wire anemometry can produce an error of 100% as the hot probe creates its own convection. Laser Doppler velocimetry allows non-impeding measurement of low velocities but only at one point at a time.

To resolve those problems, we are developing a 3D particle tracking system with millimetric particles. Each particle is to be individually followed and its 3D locations and velocities calculated. After presenting some previous works on particle velocimetry in the air, we will explain the theory of our method. Then, we will present the hardware, then the software and the first results obtained.

2. LITERATURE REVIEW

Most existing methods currently searched are based on holographic PIV (particle image velocimetry), tomographic PIV, stereographic PIV, particle streak velocimetry and particle tracking velocimetry.

Holographic PIV (HPIV) is based on the recording of the seeded flow on a hologram and the interrogation of the reconstructed image at many different times to determine the flow velocity. However, HPIV requires optical equipment including lenses, lasers and polarizers whose manipulation and calibration are very delicate. What is more, the holograms have to be chemically treated before the 3D reconstruction. Their manipulation is another source of error. This is the reason why it is very difficult to produce enough holograms and within a time short enough to yield turbulence statistics or to adapt HPIV to industry (Schnars and Juptner 1994).

In Tomographic PIV, tracer particles within the measurement volume are illuminated by a pulsed light source and the scattered light pattern is recorded simultaneously from several viewing directions using CCD cameras. The 3D particle distribution is then reconstructed as a 3D light intensity distribution, from its projections on the CCD arrays. Tomo-PIV features two major disadvantages: First, the reconstruction problem is not straightforward and it is in general underdetermined meaning that a single set of projections can result from many different 3D objects. Second, the laser light sheet is only a few mm wide (Elsinga et al. 2005), which is not suitable for our application.

Stereo PIV which is widely perceived as the 3D extension of PIV (David and Gicquel 2006). It is a geometrical reconstruction of the third velocity component from the particles' displacement within a thin laser sheet a few millimetres wide, viewed from two different angles. But the velocity of the particles situated outside the laser sheet is not calculated. Sun and Zhang (2003) measured the airflow field by using helium filled soap bubbles of 2-3mm diameter as tracers. A total of 7200 W of light was used to illuminate the tracers. Particles were captured by two CCD digital cameras placed on the same plane with an angle of 90° between the two optical axes. With a specially designed algorithm they measured particle's streak. Knowing the time of exposure, the velocity was calculated.

Their method gave good results but many problems had yet to be tackled. First of all, the light sheet created by halogen lamps, though 5.5m wide and 2.4m high, was only 6.5cm deep which means that the full-scale flow field was not really measured. Another problem is that many particles streaks are bowed, especially where turbulence takes place. Therefore, some corrective algorithms have to be applied which is a new source of error.

Scholzen and Moser (1996) developed a three-dimensional particle streak velocimetry system. In their study, three photographic cameras, a 120 mm thick white light sheet, and a digital image processing program were employed to acquire the particle streak image and extract particle displacement information. One of the three cameras with a relatively short exposure time setting was used to recognize the particle streak direction. The other two cameras, which had the same settings but were put in different locations, formed stereoscopic photographs to obtain the three components of the velocity vectors. They tracked particles in ventilated spaces up to 2.5m (L) x1.7m (H) but the depth of the processed field was only 12cm.

Particle tracking velocimetry rests on the identification and the tracking of individual particles localised thanks to an observation system from cameras laid out according to 3 or four different directions. Some particles can be recreated artificially (Schimpf et al. 2003). One of the defects of the method is the difficulty in finding the particles which overlap when the densities of sowing are strong. Densities thus have to be maintained low, typically about 0.005 particles per pixel for a system with three cameras (Maas et al. 1993). This leads to a weak space resolution speed. Maas (1992) succeeded in tracking up to 1000 individual particles in a 80mm-deep zone of interest. The identification of particles was based on the intersection of epipolar lines on at least 3 cameras arranged in a stereoscopic configuration or arranged in a way that their projective centres laid on a straight line. Many ambiguities still remained as many particle images were overlapping, leading to false candidates particles.

3. MATHEMATICAL MODEL

3.1 Distortion model

The distortion model described hereafter is called the "Plumb Bob" model (radial polynomial + "thin prism") and was first

introduced by Brown (1966). The tangential distortion is caused by imperfect centering of the lens components and other manufacturing defects in a compound lens. Let be:
f : The focal length in pixels (2x1 vector).
cc: The vector of principal point coordinates (2x1 vector).
β: The skew coefficient defining the angle between the x and y pixel axes (scalar).
k: The vector of image radial and tangential distortion coefficients (5x1 vector).

Let P be a real world point whose coordinates in the camera reference frame are $[X_c;Y_c;Z_c]$. Let be $x_n = [x, y]$ the normalized projection of this point on the image plane according to the intrinsic parameters (f, cc, β, k). Normalized coordinates are defined as the pinhole projection coordinates obtained using a unit focal length. For example, let be xr the image coordinates of a real point P then xn= - xr/f. So we can write:

$$\begin{bmatrix} x \\ y \end{bmatrix} = \begin{bmatrix} X_c / Z_c \\ Y_c / Z_c \end{bmatrix} \quad (1)$$

Let $r^2=x^2+y^2$. After including lens distortion, the new normalized point coordinate x_d is defined as follows:

$$\overrightarrow{x_d} = (1 + k_1.r^2 + k_2.r^4 + k_5.r^6)\overrightarrow{x_n} + \overrightarrow{dx} \quad (2)$$

where dx is the tangential distortion vector:

$$\overrightarrow{dx} = \begin{bmatrix} 2k_3.x.y + k_4.(r^2 + 2x^2) \\ 2k_4.x.y + k_3.(r^2 + 2y^2) \end{bmatrix} \quad (3)$$

After applying the distortion, the final pixel coordinates x_{pixel} of the projection of P on the image plane reads:

$$\overrightarrow{x_{pixel}} = \begin{bmatrix} x_p \\ y_p \end{bmatrix} = \begin{bmatrix} fc_1.(x_{d1} + \beta.x_{d2}) + cc_1 \\ fc_2.x_{d2} + cc_2 \end{bmatrix} \quad (4)$$

3.2 Triangulation

Let be R and T respectively the rotation and translation matrix which transform camera frame coordinates $XX_c = [X_c;Y_c;Z_c]$ into real world coordinates XX = [X;Y;Z]. Matrix R and T are extrinsic parameters given by calibration.

$$XXc = R*XX + T \quad (5)$$

Equation (1) and (5) give:

$$\begin{cases} x = \dfrac{R_{11}X + R_{12}Y + R_{13}Z + T_1}{R_{31}X + R_{32}Y + R_{33}Z + T_3} \\ y = \dfrac{R_{21}X + R_{22}Y + R_{23}Z + T_2}{R_{31}X + R_{32}Y + R_{33}Z + T_3} \end{cases} \quad (6)$$

The same model is applied to the other two cameras, every parameter varying from one camera to another, including matrix R and T. Thus is provided an overdeterminated system of six equations for 3 unknowns (X,Y,Z), which is solved using a least squares method.

4. EXPERIMENTAL SETUP

4.1 Particle seeding system

The air in the room is seeded with helium filled soap bubbles. The use of buoyant bubbles as flow tracers in air has been investigated by Kerho and Bragg (1994). The bubble generator (Fig.1) removes the bubbles that are heavier or lighter than air (Anonymous 1988). The bubbles have a diameter of 2-3mm which is an adequate size for visualization of centimetric phenomena.

To avoid any disturbance of the air by the generator, it is stopped 20 seconds before starting the measurement. The bubbles can last around 2 minutes in mid air, and do not explode when colliding into walls or equipment. Maximum generation rates is 400 bubbles/s.

Figure 1. Bubble generator.

4.2 Acquisition system

We use three Dalsa 4M 60 CMOS digital video cameras. Their resolution is 2352*1728 pixels. Thus, in a $2m^3$ scene, each bubble is approximately captured by 1 pixel. Their frame rate can be varied from 30 to 400 frames per second, which is suitable for air velocity visualization in rooms. Each video camera is mounted with an additional large angle fix lens in order to cope with the feeble recoil available in the room. The cameras are placed along 3 different planes (Fig. 2).

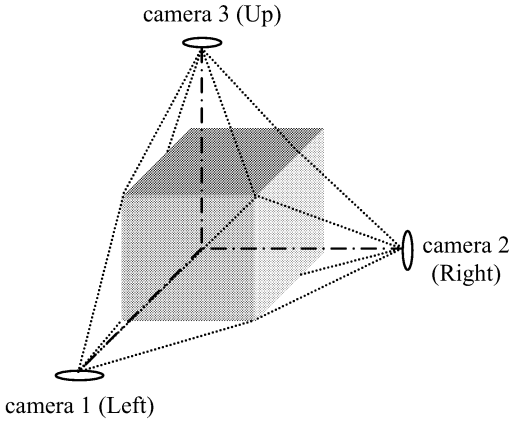

Figure 2. Cameras locations and field of vision.

4.3 Calibration target

Each digital video camera is calibrated using a planar checkerboard composed of black and white 30mm-large squares. The checkerboard has 12 horizontal squares and 8 vertical squares. Border squares were not considers during calibration. The process of calibrating allows to recover the intrinsic and extrinsic parameters of each camera.

4.4 Illumination system

It is composed of 8 Balcar Quadlite lamps. Due to fluorescent technology, each 250W lamp actually produces an equivalent of 1000W and 8300 candelas. Each lamp is equipped with 8 mobile mirror reflectors and a tilted grid placed in front of the bulbs so as to uniformly diffuse light towards any chosen direction. The angle of inclination of grids is either 45° or 60°.

The lamps are placed behind the glass-panelled side of the test room to avoid interference with air motion due to heat generation. The eight of them form a rectangular pattern in order to reproduce the ring-shaped flash of modern digital cameras. We noticed that to be visible, the bubbles have to be illuminated in back reflection which means that the light must come from behind each camera while the wall facing each camera must remain somber.

4.5 The test room

The experiment is taking place in a $3.1*3.1*2.5m^3$ (W*D*H) test room whose boundary conditions and inner values like temperature, air velocity and solar radiation can be imposed and monitored. Air velocity is currently calculated in the test room using hot wire anemometry. The test room has a glass-panelled side. Other walls are grey, including soil and ceiling.

5. PARTICLE TRACKING ALGORITHM

After calibration of cameras and image acquisistion, the tracking process follows three main steps:

5.1. Detection of particles and calculation pixel coordinates

The background of the images is cluttered with hot-wire anemometry, temperature, humidity and radiation measurement instrumentation in the test room. The luminance of the background is first slightly increased to cope with the frequency variations of light. Then the background is subtracted from each image and the resulting image is binarised.

A low-pass filtering is applied to remove overlarge speckles created by bubbles outside the common field of view. This is done by using a disk-shaped structuring element of radius the same pixel radius as particles. Then, pixel coordinates are automatically calculated as the centers of mass of the remaining speckles.

5.2 Establishment of correspondences

Bubbles are very small and homogenous. Besides, the field of interest is very deep. Therefore, an image-domain correspondence have been discarded. Instead, the centroids' pixel coordinates in each view are sorted based on the

real world coordinates of combinatory possible solutions. The 3D coordinates are calculated using 2 cameras at a time. Let us consider Table 1 as an example:

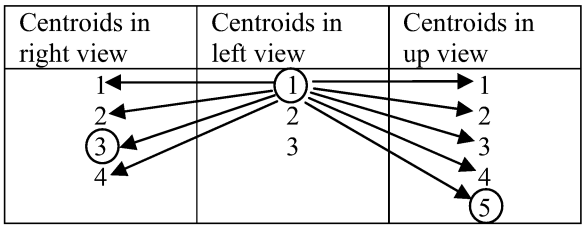

Table 1. Illustration of the identification algorithm process.

If real world coordinates calculated with couple of centroids (1,3) and couple (1,5) are ''similar'', then centroids 3, 1 and 5 are images of the same bubble. The similarity criteria is defined as the minimum of Euclidian distance among every other 3D coordinates. $A_i(x_a,y_a,z_a)$ and $B_j(x_b,y_b,z_b)$ being two real world coordinates, we look for:

$$\min_{i,j}\left(\left\|A_i-B_j\right\|_2\right)=\min_{i,j}\left(\sqrt{\left|x_a-x_b\right|^2+\left|y_a-y_b\right|^2+\left|z_a-z_b\right|^2}\right) \quad (7)$$

where $||\ ||_2$ is the 2-norm. Even if this procedure allow us to improve the depth of measurement, it does not completely prevent occlusion problems.

5.3 Tracking in object and image space.

The tracking is done by cross correlation. The interrogation windows sampled on the three images of instant t consist of square matrix framing each bubble. The pixel length of those matrix is 2*r where r is the maximum pixel radius of a bubble. The research windows sampled on images at instant t+1 consist of matrix centered on the previous location of bubbles at images t. The length of research windows matrix is 2*α with:

$$\alpha=\frac{V_{\max}.t}{n}+r \quad (8)$$

where
V_{max} : Estimated maximum velocity of a bubble
t: Time space between two successive images
n: Length of one pixel (m/pixel)

The erroneous vectors are eliminated using a time-based smoothing procedure: Let B be the 3D coordinates of a bubble, t an instant and s a chosen threshold:

$$\left|\left\|B(t)\right\|-\frac{\left\|B(t-1)\right\|+\left\|B(t+1)\right\|}{2}\right|\succ s$$

$$\Rightarrow B(t)=\frac{B(t-1)+B(t+1)}{2}$$

6. VALIDATION

A single table tennis ball was moved on eleven precisely located places separated by precisely measured distances. The difference between algorithm and measurement was +1.556mm, -1.533mm, and + 1.662mm respectively for the x, y and z coordinates. The remaining error is mainly due to the refractive index changes through the camera glass window according to Snell's law, to pixel errors during calibration and to sensors misalignment. The misalignment of video cameras 4M60'lenses was ±0.1mm for x and y directions and ±0.25mm for z direction with a tilt angle of 0.2°. Bubbles were also issued from a tailpipe with known velocity. Difference between algorithm and hot-wire anemometry at the pipe nozzle was - 0.021m/s.

7. RESULTS

Images of bubbles spurting out from a pipe where taken at the speed of 60 frames/s .

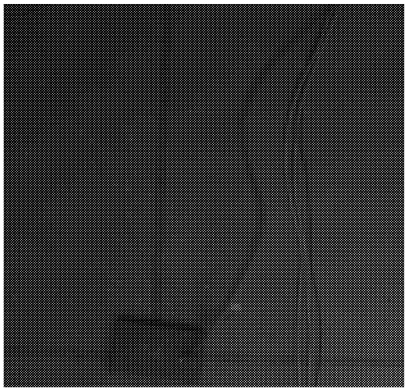

Up view image

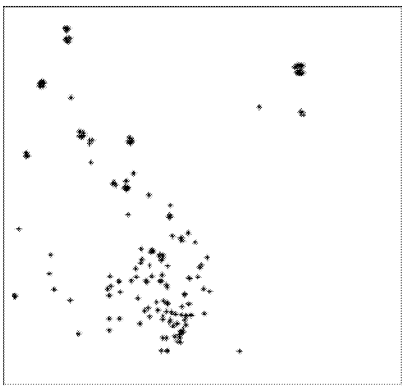

Up view centroids

Figure 4. Image of bubbles spurting out from a pipe taken by the up camera and result of the detection process.

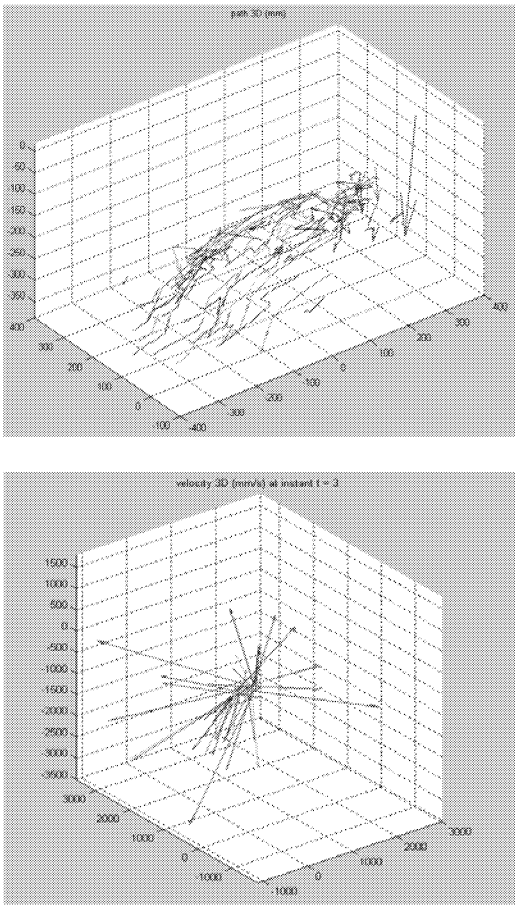

Figure 5. 3D path and velocity of the bubbles at instant t=3 (from the third triplet of images).

7. PERSPECTIVES OF RESEARCH.

The next step of the research will consist in taking into account the particles entering the field of vision after the initialisation process of the tracking. Algorithms such as Chetverikov and Verestoy's (1998) seem promising.

We are considering the comparison of the system's results with traditional 2D PIV. To improve speed, we are also considering implementation of the algorithm on Graphic Processor Units platforms. After enlargement of the field of interest by using more cameras, the system may be fit for the research on convective heat transfers and pollutants displacements in full scale rooms.

REFERENCES

Anonymous (1988). SAI Bubble Generator: Description and Operating Instructions. Sage Action, Inc., New-York.

Brown D.C. (1966). Decentering distortion of lenses. Photogrammetric engeenering 32(3):444-462.

Chetverikov D., Verestoy J. (1998). Tracking Feature Points: a New Algorithm. Computer and Automation Research Institute Budapest, Kende u.13-17, H-1111. Hungary.

David L. Gicquel P. (2006). Évolution de la technique PIV à travers quelques conférences internationales de 2000 à aujourd'hui. Congrès Francophone de Techniques Laser, CFTL 2006, Toulouse, sept. 19-22.

Elsinga G. et al. (2005). Assessment of Tomo-PIV for three dimensional flows, 6th International Symposium on PIV, Pasadena, USA, september 21-23.

Kerho M.F., Bragg M.B. (1994). Neutrally buoyant bubbles used as flow tracers in air. Experiments in Fluids, 16:393.400.

Maas H.G. (1992). Complexity analysis for the establishment of image correspondences of dense spatial target fields, International Advances of Photogrammetry and Remote Sensing, XXIX(B5): 102.107.

Maas H.G. et al. (1993). Particle tracking velocimetry in three-dimensional flows. *Exp. Fluids*, vol. 15, pp.133-146.

Schimpf A. et al. (2003). Photogrammetric particle image velocimetry, 5th International Symposium on Particle Image Velocimetry, Busan, Korea, paper 3115.

Schnars U., Juptner W. (1994). Direct recording of holograms by a CCD target and numerical reconstruction. Applied Optics, Vol. 33, 2: p.179.

Scholzen F., Moser A. (1996) Three-dimensional particle streak velocimetry for room air flows with automatic stereo-photogrammetric image processing. Roomvent, pp. 555-562.

Sun Y., Zhang Y. (2003). Development of a stereoscopic particle image velocimetry system for full-scale room airflow studies, Part II: experimental setup. Transactions of American Society of Heating, Refrigerating and Air conditioning Engineering, 09(2), pp. 540-548.